

January 26, 2023

A Comparative Study of Dark Energy Constraints from Current Observational Data

Yun Wang^{1*}, Chia-Hsun Chuang¹, & Pia Mukherjee²¹*Homer L. Dodge Department of Physics & Astronomy,
Univ. of Oklahoma, 440 W Brooks St., Norman, OK 73019*²*Sussex Astronomy Centre, Dept. of Physics & Astronomy,
University of Sussex, Falmer, Brighton, BN1 9QH, U.K.*

We examine how dark energy constraints from current observational data depend on the analysis methods used: the analysis of Type Ia supernovae (SNe Ia), and that of galaxy clustering data. We generalize the flux-averaging analysis method of SNe Ia to allow correlated errors of SNe Ia, in order to reduce the systematic bias due to weak lensing of SNe Ia. We find that flux-averaging leads to larger errors on dark energy and cosmological parameters if only SN Ia data are used. When SN Ia data (the latest compilation by the SNLS team) are combined with WMAP 7 year results (in terms of our Gaussian fits to the probability distributions of the CMB shift parameters), the latest Hubble constant (H_0) measurement using the Hubble Space Telescope (HST), and gamma ray burst (GRB) data, flux-averaging of SNe Ia increases the concordance with other data, and leads to significantly tighter constraints on the dark energy density at $z = 1$, and the cosmic curvature Ω_k . The galaxy clustering measurements of $H(z = 0.35)r_s(z_d)$ and $r_s(z_d)/D_A(z = 0.35)$ (where $H(z)$ is the Hubble parameter, $D_A(z)$ is the angular diameter distance, and $r_s(z_d)$ is the sound horizon at the drag epoch) by Chuang & Wang (2011) are consistent with SN Ia data, given the same priors (CMB+ H_0 +GRB), and lead to significantly improved dark energy constraints when combined. Current data are fully consistent with a cosmological constant and a flat universe.

PACS numbers: 98.80.Es, 98.80.-k, 98.80.Jk

Keywords: Cosmology

I. INTRODUCTION

Solving the mystery of cosmic acceleration [1, 2] is one of the most important challenges in cosmology today. Current observational data are not sufficient for differentiating two likely explanations for the observed cosmic acceleration: dark energy, and the modification of general relativity. For recent reviews, see [3–10].

There are a number of powerful direct probes of dark energy: Type Ia supernovae (SNe Ia) [1, 2]; galaxy clustering (GC), especially the baryon acoustic oscillations (BAO) [11, 12]; and weak lensing of galaxies [13, 14]. These methods are complementary to each other, and each method has its own systematic uncertainties. Other data, e.g., gamma ray bursts [15–17], can help strengthen the dark energy constraints.

The cosmic microwave background (CMB) anisotropy data provide strong priors on cosmological parameters (see, e.g., [18]). Direct measurements on the Hubble constant (see, e.g., [19]) also help break the degeneracy amongst the dark energy and cosmological parameters.

Much progress has been made since the discovery of cosmic acceleration in 1998. However, current data are still rather limited in constraining dark energy. In particular, different analysis methods of the same data could lead to significantly different constraints on dark energy. This is probably due to the fact that different methods

have different residual systematic biases, and they often assume different priors on cosmological parameters as well.

In this paper we examine these issues by studying how dark energy constraints from current observational data depend on the analysis methods used. In particular, we explore the impact on the overall dark energy constraints of (1) using flux-averaging to minimize the weak lensing bias in the analysis of SNe Ia; (2) using radial and transverse distance constraints derived from GC data without assuming CMB priors.

We describe our method in Sec.II, present our results in Sec.III, and conclude in Sec.IV.

II. METHOD

We only use methods that give geometric constraints on dark energy. The constraints on the growth rate of cosmic large scale structure are degenerate with the geometric constraints (see, e.g., [20, 21]); current data do not allow the determination of both without strong assumptions, e.g., assuming that general relativity is not modified.

Geometric constraints on dark energy are derived from the measurement of distances. The comoving distance to an object at redshift z is given by:

$$r(z) = cH_0^{-1} |\Omega_k|^{-1/2} \text{sinn}[|\Omega_k|^{1/2} \Gamma(z)], \quad (1)$$

$$\Gamma(z) = \int_0^z \frac{dz'}{E(z')}, \quad E(z) = H(z)/H_0$$

*email: wang@nhn.ou.edu

where $\text{sinn}(x) = \sin(x)$, x , $\sinh(x)$ for $\Omega_k < 0$, $\Omega_k = 0$, and $\Omega_k > 0$ respectively; and the expansion rate of the universe $H(z)$ (i.e., the Hubble parameter) is given by

$$H^2(z) \equiv \left(\frac{\dot{a}}{a}\right)^2 \quad (2)$$

$$= H_0^2 [\Omega_m(1+z)^3 + \Omega_r(1+z)^4 + \Omega_k(1+z)^2 + \Omega_X X(z)]$$

where $\Omega_m + \Omega_r + \Omega_k + \Omega_X = 1$, and the dark energy density function $X(z)$ is defined as

$$X(z) \equiv \frac{\rho_X(z)}{\rho_X(0)}. \quad (3)$$

Note that $\Omega_r \ll \Omega_m$, thus the Ω_r term is usually omitted in dark energy studies, since dark energy should only be important at late times.

A. Analysis of SN Ia Data

SN Ia data give measurements of the luminosity distance $d_L(z)$ through that of the distance modulus of each SN:

$$\mu_0 \equiv m - M = 5 \log \left[\frac{d_L(z)}{\text{Mpc}} \right] + 25, \quad (4)$$

where m and M represent the apparent and absolute magnitude of a SN. The luminosity distance $d_L(z) = (1+z)r(z)$, with the comoving distance $r(z)$ given by Eq.(1).

We use the compilation of SN Ia data by Conley et al. (2011) [22], which include the SNe Ia from the first three years of the Supernova Legacy Survey (SNLS3), the largest homogeneous SN Ia data set. We compare two methods for using these SNe in constraining dark energy: with flux-averaging of SNe Ia, and without.

1. SN Ia Data

For a set of 472 SNe Ia, Conley et al. (2011) [22] give the apparent B magnitude, m_B , and the covariance matrix for $\Delta m \equiv m_B - m_{\text{mod}}$, with

$$m_{\text{mod}} = 5 \log_{10} \mathcal{D}_L(z|\mathbf{s}) - \alpha(s-1) + \beta\mathcal{C} + \mathcal{M}, \quad (5)$$

where $\mathcal{D}_L(z|\mathbf{s})$ is the luminosity distance multiplied by H_0 for a given set of cosmological parameters $\{\mathbf{s}\}$, s is the stretch measure of the SN light curve shape, and \mathcal{C} is the color measure for the SN. \mathcal{M} is a nuisance parameter representing some combination of the absolute magnitude of a fiducial SN Ia, M , and the Hubble constant H_0 . Since the time dilation part of the observed luminosity distance depends on the total redshift z_{hel} (special relativistic plus cosmological), we have [23]

$$\mathcal{D}_L(z|\mathbf{s}) \equiv c^{-1} H_0 (1 + z_{\text{hel}}) r(z|\mathbf{s}), \quad (6)$$

where z and z_{hel} are the CMB restframe and heliocentric redshifts of the SN.

For a set of N SNe with correlated errors, we have [22]

$$\chi^2 = \Delta \mathbf{m}^T \cdot \mathbf{C}^{-1} \cdot \Delta \mathbf{m} \quad (7)$$

where $\Delta \mathbf{m}$ is a vector with N components, and \mathbf{C} is the $N \times N$ covariance matrix of the SNe Ia.

Note that Δm is equivalent to $\Delta \mu_0$, since

$$\Delta m \equiv m_B - m_{\text{mod}} = [m_B + \alpha(s-1) - \beta\mathcal{C}] - \mathcal{M}. \quad (8)$$

The total covariance matrix is [22]

$$\mathbf{C} = \mathbf{D}_{\text{stat}} + \mathbf{C}_{\text{stat}} + \mathbf{C}_{\text{sys}}, \quad (9)$$

with the diagonal part of the statistical uncertainty given by [22]

$$\begin{aligned} \mathbf{D}_{\text{stat},ii} &= \sigma_{m_B,i}^2 + \sigma_{\text{int}}^2 + \sigma_{\text{lensing}}^2 + \sigma_{\text{host correction}}^2 \\ &+ \left[\frac{5(1+z_i)}{z_i(1+z_i/2) \ln 10} \right]^2 \sigma_{z,i}^2 + \alpha^2 \sigma_{s,i}^2 + \beta^2 \sigma_{\mathcal{C},i}^2 \\ &+ 2\alpha C_{m_B s,i} - 2\beta C_{m_B \mathcal{C},i} - 2\alpha\beta C_{s\mathcal{C},i}, \end{aligned} \quad (10)$$

where $C_{m_B s,i}$, $C_{m_B \mathcal{C},i}$, and $C_{s\mathcal{C},i}$ are the covariances between m_B , s , and \mathcal{C} for the i -th SN. Note also that $\sigma_{z,i}^2$ includes a peculiar velocity residual of 0.0005 (i.e., 150 km/s) added in quadrature [22].

The statistical and systematic covariance matrices, \mathbf{C}_{stat} and \mathbf{C}_{sys} , are generally not diagonal [22], and are given in the form:

$$\mathbf{C}_{\text{stat}} + \mathbf{C}_{\text{sys}} = V_0 + \alpha^2 V_a + \beta^2 V_b + 2\alpha V_{0a} - 2\beta V_{0b} - 2\alpha\beta V_{ab}. \quad (11)$$

where V_0 , V_a , V_b , V_{0a} , V_{0b} , and V_{ab} are matrices given by the SNLS data archive at <https://tspace.library.utoronto.ca/handle/1807/24512/>. \mathbf{C}_{stat} includes the uncertainty in the SN model. \mathbf{C}_{sys} includes the uncertainty in the zero point. Note that \mathbf{C}_{stat} and \mathbf{C}_{sys} do not depend on \mathcal{M} , since the relative distance moduli are independent of the value of \mathcal{M} [22].

We refer the reader to Conley et al. (2011) [22] for a detailed discussion of the origins of the statistical and systematic errors. As an example, we note that the correlation of errors on different SNe arises from a statistical uncertainty in the zero point of one passband, e.g., r_M . This directly affects all SNe with r_M measurements due to K-corrections (restframe B to r_M), and indirectly affects even the SNe without r_M measurements through the empirical SN models by changing the templates and the measured color-luminosity relationship.

2. The Recipe for Flux-Averaging of SNe Ia

Flux-averaging of SNe Ia was proposed to reduce the effect of the weak lensing of SNe Ia on cosmological parameter estimation [24]. The basic idea is that because of flux conservation in gravitational lensing, the average

magnification of a large number of SNe Ia at the same redshift should be unity. Thus averaging the observed flux from a large number of SNe Ia at the same redshift can recover the unlensed brightness of the SNe Ia at that redshift.

Wang & Mukherjee (2004) [25] and Wang (2005) [26] developed a consistent framework for flux-averaging SNe Ia. Wang & Mukherjee (2004) [25] gave the recipe for flux-averaging SNe Ia in the absence of correlated errors. Here we modify and generalize the recipe to allow correlated errors of SNe Ia.

As described in [24], the fluxes of SNe Ia in a redshift bin should only be averaged *after* removing their redshift dependence, which is a model-dependent process. For χ^2 statistics using MCMC or a grid of parameters, here are the steps in flux-averaging:

(1) Convert the distance modulus of SNe Ia into “fluxes”,

$$F(z_l) \equiv 10^{-(\mu_0^{\text{data}}(z_l) - 25)/2.5} = \left(\frac{d_L^{\text{data}}(z_l)}{\text{Mpc}} \right)^{-2}. \quad (12)$$

(2) For a given set of cosmological parameters $\{\mathbf{s}\}$, obtain “absolute luminosities”, $\{\mathcal{L}(z_l)\}$, by removing the redshift dependence of the “fluxes”, i.e.,

$$\mathcal{L}(z_l) \equiv d_L^2(z_l|\mathbf{s}) F(z_l). \quad (13)$$

(3) Flux-average the “absolute luminosities” $\{\mathcal{L}_l^i\}$ in each redshift bin i to obtain $\{\bar{\mathcal{L}}^i\}$:

$$\bar{\mathcal{L}}^i = \frac{1}{N_i} \sum_{l=1}^{N_i} \mathcal{L}_l^i(z_l^{(i)}), \quad \bar{z}_i = \frac{1}{N_i} \sum_{l=1}^{N_i} z_l^{(i)}. \quad (14)$$

(4) Place $\bar{\mathcal{L}}^i$ at the mean redshift \bar{z}_i of the i -th redshift bin, now the binned flux is

$$\bar{F}(\bar{z}_i) = \bar{\mathcal{L}}^i / d_L^2(\bar{z}_i|\mathbf{s}). \quad (15)$$

(5) Compute the covariance matrix of $\bar{F}(\bar{z}_i)$ and $\bar{F}(\bar{z}_j)$:

$$\begin{aligned} & \text{Cov} [\bar{F}(\bar{z}_i), \bar{F}(\bar{z}_j)] \\ &= \frac{1}{N_i N_j} \left[\frac{\ln 10 / 2.5}{d_L(\bar{z}_i|\mathbf{s}) d_L(\bar{z}_j|\mathbf{s})} \right]^2 \\ & \quad \sum_{l=1}^{N_i} \sum_{m=1}^{N_j} \mathcal{L}(z_l^{(i)}) \mathcal{L}(z_m^{(j)}) \langle \Delta \mu_0^{\text{data}}(z_l^{(i)}) \Delta \mu_0^{\text{data}}(z_m^{(j)}) \rangle \end{aligned} \quad (16)$$

where $\langle \Delta \mu_0^{\text{data}}(z_l^{(i)}) \Delta \mu_0^{\text{data}}(z_m^{(j)}) \rangle$ is the covariance of the measured distance moduli of the l -th SN Ia in the i -th redshift bin, and the m -th SN Ia in the j -th redshift bin. $\mathcal{L}(z)$ is defined by Eqs.(12) and (13).

(6) For the flux-averaged data, $\{\bar{F}(\bar{z}_i)\}$, compute

$$\chi^2 = \sum_{ij} \Delta \bar{F}(\bar{z}_i) \text{Cov}^{-1} [\bar{F}(\bar{z}_i), \bar{F}(\bar{z}_j)] \Delta \bar{F}(\bar{z}_j) \quad (17)$$

where

$$\Delta \bar{F}(\bar{z}_i) \equiv \bar{F}(\bar{z}_i) - F^p(\bar{z}_i|\mathbf{s}), \quad (18)$$

with $F^p(\bar{z}_i|\mathbf{s}) = (d_L(z|\mathbf{s})/\text{Mpc})^{-2}$.

For the sample of SNe we use in this study, we flux-averaged the SNe with $dz = 0.07$, to ensure that all redshift bins contain at least one SN. Our SN flux-averaging code is available at <http://www.nhn.ou.edu/~wang/SNcode/>.

B. Galaxy Clustering Data

For GC data, we use the distance measurements from the SDSS DR7 data. We compare two sets of distance measurements from SDSS DR7: (1) “CW2”: the measurement of $H(z)r_s(z_d)$ and $r_s(z_d)/D_A(z)$ (where $H(z)$ is the Hubble parameter, $D_A(z)$ is the angular diameter distance, and $r_s(z_d)$ is the sound horizon at the drag epoch) by Chuang & Wang (2011) [27] from the two-dimensional two-point correlation function of SDSS DR7 Luminous Red Galaxies (LRGs); (2) “WP2”: the measurement of $r_s(z_d)/D_V(z = 0.2)$ and $r_s(z_d)/D_V(z = 0.35)$ (where $D_V(z)$ is the spherically-averaged distance) by Percival et al. (2010) [28] from the spherically-averaged power spectrum of combined data of SDSS DR7 LRG and main galaxy samples and 2-degree Field Galaxy Redshift Survey (2dFGRS).

Using the two-dimensional two-point correlation function of SDSS DR7 in the scale range of 40-120 Mpc/ h , Chuang & Wang (2011) [27] found that

$$\begin{aligned} H(z = 0.35)r_s(z_d) &= 13020 \pm 530 \text{ km/s (4\%)} \\ r_s(z_d)/D_A(z = 0.35) &= 0.1518 \pm 0.0062 \text{ (4\%)} \\ r &= -0.0584, \end{aligned} \quad (19)$$

where r is the normalized correlation coefficient between $H(z = 0.35)r_s(z_d)$ and $r_s(z_d)/D_A(z = 0.35)$, and $r_s(z_d)$ is the sound horizon at the drag epoch (given by Eqs.(28) and (32). The inverse covariance matrix of $H(z = 0.35)r_s(z_d)$ and $r_s(z_d)/D_A(z = 0.35)$ is

$$C_{\text{GC,CW2}}^{-1} = \begin{pmatrix} 0.35722E - 05 & 0.17833E - 01 \\ 0.17833E - 01 & 0.26104E + 05 \end{pmatrix} \quad (20)$$

Spherically-averaged data give a measurement of $d_z \equiv r_s(z_d)/D_V(z)$, with

$$D_V(z) \equiv \left[\frac{r(z)^2 cz}{H(z)} \right]^{1/3}. \quad (21)$$

Chuang & Wang (2011) found that

$$d_{0.35}^{\text{CW}} \equiv r_s(z_d)/D_V(z = 0.35) = 0.1161 \pm 0.0034 \text{ (2.9\%)} \quad (22)$$

from the spherically-averaged correlation function of SDSS LRGs.

Using the spherically-averaged power spectrum of combined data of SDSS DR7 LRG and main galaxy samples and 2dFGRS, Percival et al. (2010) [28] found that

$$\begin{aligned} d_{0.2}^{WP} &\equiv r_s(z_d)/D_V(z=0.2) = 0.1905 \pm 0.0061 \text{ (3.2\%)} \\ d_{0.35}^{WP} &\equiv r_s(z_d)/D_V(z=0.35) = 0.1097 \pm 0.0036 \text{ (3.3\%)} \\ r &= 0.337, \end{aligned} \quad (23)$$

where r is the normalized correlation coefficient of $d_{0.2}$ and $d_{0.35}$. The inverse covariance matrix of $(d_{0.2}, d_{0.35})$ is [28]

$$C_{GC,WP}^{-1} = \begin{pmatrix} 30124 & -17227 \\ -17227 & 86977 \end{pmatrix} \quad (24)$$

For comparison, we also consider the distance measurements from the WiggleZ survey at $z = 0.6$ by Blake et al. (2011) [29], and from the 6dF GRS at $z = 0.106$ by Beutler et al. (2011) [30]:

$$\begin{aligned} d_{0.6} &\equiv r_s(z_d)/D_V(z=0.6) = 0.0692 \pm 0.0033 \\ d_{0.106} &\equiv r_s(z_d)/D_V(z=0.106) = 0.336 \pm 0.015 \end{aligned} \quad (25)$$

GC data are included in our analysis by adding the following term to the χ^2 of a given model with

$$\chi_{GC}^2 = \Delta p_i [C_{GC}^{-1}(p_i, p_j)] \Delta p_j, \quad \Delta p_i = p_i - p_i^{data}. \quad (26)$$

For the Chuang & Wang (2011) GC measurements [27], $p_1 = H(z=0.35)r_s(z_d)$ and $p_2 = r_s(z_d)/D_A(z=0.35)$. For the Percival et al. (2010) GC measurements [28], $p_1 = d_{0.2}$ and $p_2 = d_{0.35}$. Note that p_i^{data} ($i = 1, 2$) are given in Eqs.(19) and (23), and the inverse covariance matrices are given in Eqs.(20) and (24). Since the WiggleZ and 6dF surveys give independent measurements, Eq.(26) is replaced with $\chi_{GC}^2 = \sum_{i=1}^2 (\Delta p_i)^2 / \sigma_{p_i}^2$, with $p_1 = d_{0.6}$, and $p_2 = d_{0.106}$, and σ_{p_i} ($i = 1, 2$) given in Eq.(25).

C. CMB data

CMB data give us the comoving distance to the photon-decoupling surface $r(z_*)$, and the comoving sound horizon at photo-decoupling epoch $r_s(z_*)$ [31]. Wang & Mukherjee 2007 [32] showed that the CMB shift parameters

$$R \equiv \sqrt{\Omega_m H_0^2} r(z_*), \quad l_a \equiv \pi r(z_*)/r_s(z_*), \quad (27)$$

together with $\omega_b \equiv \Omega_b h^2$, provide an efficient summary of CMB data as far as dark energy constraints go. This has been verified by [33]. Using $\{R, l_a, \omega_b\}$ is equivalent to using $\{R, l_a, z_*\}$ as CMB distance priors [34].

The comoving sound horizon at redshift z is given by

$$\begin{aligned} r_s(z) &= \int_0^t \frac{c_s dt'}{a} = cH_0^{-1} \int_z^\infty dz' \frac{c_s}{E(z')}, \\ &= cH_0^{-1} \int_0^a \frac{da'}{\sqrt{3(1 + \bar{R}_b a') a'^4 E^2(z')}}, \end{aligned} \quad (28)$$

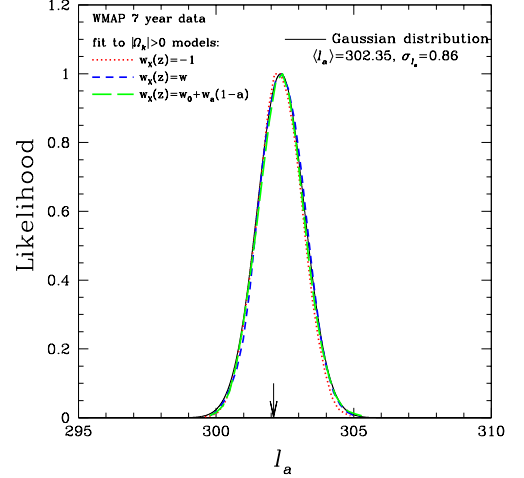


FIG. 1: One-dimensional marginalized probability distributions of CMB shift parameter l_a derived from WMAP7 data.

where a is the cosmic scale factor, $a = 1/(1+z)$, and $a^4 E^2(z) = \Omega_m(a + a_{eq}) + \Omega_k a^2 + \Omega_X X(z) a^4$, with $a_{eq} = \Omega_{rad}/\Omega_m = 1/(1+z_{eq})$, and $z_{eq} = 2.5 \times 10^4 \Omega_m h^2 (T_{CMB}/2.7 \text{ K})^{-4}$. The sound speed is $c_s = 1/\sqrt{3(1 + \bar{R}_b a)}$, with $\bar{R}_b a = 3\rho_b/(4\rho_\gamma)$, $\bar{R}_b = 31500 \Omega_b h^2 (T_{CMB}/2.7 \text{ K})^{-4}$. We take $T_{CMB} = 2.725$.

The redshift to the photon-decoupling surface, z_* , is given by the fitting formula [35]:

$$z_* = 1048 [1 + 0.00124(\Omega_b h^2)^{-0.738}] [1 + g_1(\Omega_m h^2)^{g_2}], \quad (29)$$

where

$$g_1 = \frac{0.0783 (\Omega_b h^2)^{-0.238}}{1 + 39.5 (\Omega_b h^2)^{0.763}} \quad (30)$$

$$g_2 = \frac{0.560}{1 + 21.1 (\Omega_b h^2)^{1.81}} \quad (31)$$

The redshift of the drag epoch z_d is well approximated by [36]

$$z_d = \frac{1291(\Omega_m h^2)^{0.251}}{1 + 0.659(\Omega_m h^2)^{0.828}} [1 + b_1(\Omega_b h^2)^{b_2}], \quad (32)$$

where

$$b_1 = 0.313(\Omega_m h^2)^{-0.419} [1 + 0.607(\Omega_m h^2)^{0.674}] \quad (33)$$

$$b_2 = 0.238(\Omega_m h^2)^{0.223}. \quad (34)$$

Figs.1-5 show the one-dimensional marginalized probability distributions (pdf) of $(l_a, R, z_*, n_s, r_s(z_d))$ derived from WMAP7 data, for three different assumptions about dark energy: (1) $w_X(z) = -1$; (2) $w_X(z) = w$ (constant); (3) $w_X(z) = w_0 + w_a(1-a)$ [37]. Note that these pdf's are nearly independent of the assumption about dark energy, and are well fitted by Gaussian

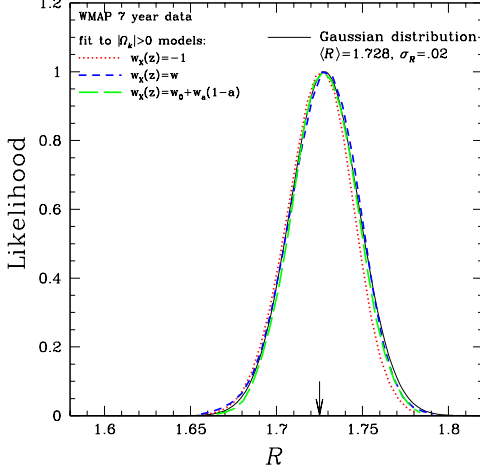


FIG. 2: One-dimensional marginalized probability distribution of CMB shift parameter R derived from WMAP7 data.

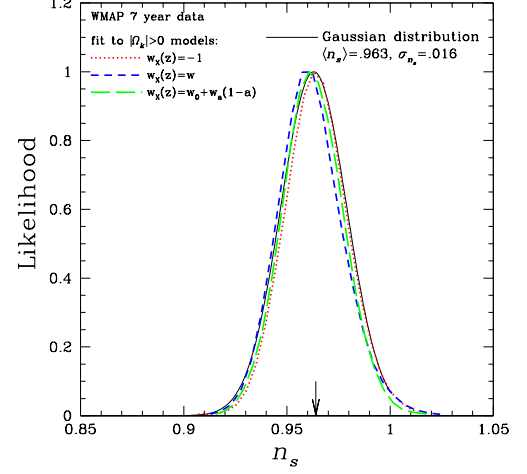


FIG. 4: One-dimensional marginalized probability distributions of powerlaw index of primordial matter power spectrum, n_s , derived from WMAP7 data.

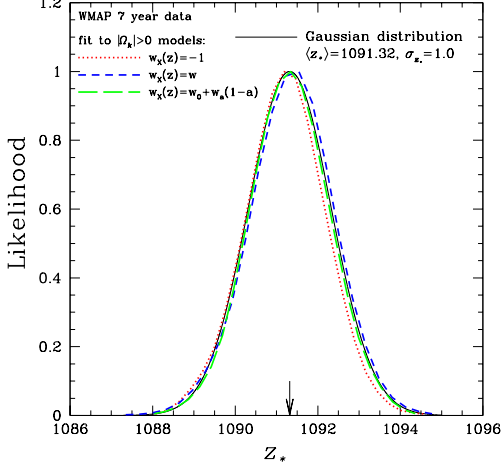


FIG. 3: One-dimensional marginalized probability distribution of the redshift to the photon-decoupling surface, z_* , derived from WMAP7 data.

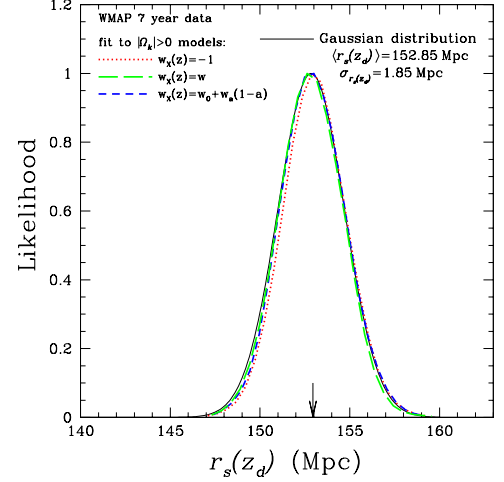


FIG. 5: One-dimensional marginalized probability distribution of the sound horizon at the drag epoch, $r_s(z_d)$, derived from WMAP7 data.

distributions with the following means and standard deviations:

$$\begin{aligned}
 \langle l_a \rangle &= 302.35, \sigma(l_a) = 0.86 \\
 \langle R \rangle &= 1.728, \sigma(R) = 0.02 \\
 \langle z_* \rangle &= 1091.32, \sigma(z_*) = 1.0 \\
 \langle n_s \rangle &= 0.963, \sigma(n_s) = 0.016 \\
 \langle r_s(z_d) \rangle &= 152.85 \text{ Mpc}, \sigma(r_s(z_d)) = 1.85 \text{ Mpc}.
 \end{aligned} \quad (35)$$

The arrows in Figs.1-5 indicate the bestfit values for a constant w from Komatsu's website [38]; they are fully consistent with our Gaussian fits.

The normalized covariance matrix of

$(l_a, R, z_*, n_s, r_s(z_d))$ is

$$\begin{pmatrix}
 1.0000 & .20794 & .47422 & -.54889 & .34914 \\
 .20794 & 1.0000 & .74409 & -.44370 & -.76929 \\
 .47422 & .74409 & 1.0000 & -.79575 & -.19121 \\
 -.54889 & -.44370 & -.79575 & 1.0000 & -.09973 \\
 .34914 & -.76929 & -.19121 & -.09973 & 1.0000
 \end{pmatrix} \quad (36)$$

We find that the addition of $r_s(z_d)$ is redundant, and amounts to partially double-weighting the CMB constraints; so its measurement cannot be used in the CMB priors unless it is used to replace $l_a(z_*)$. This was not apparent when WMAP5 data were used [39]; this is because WMAP7 data provide significantly tighter constraints on the set of CMB distance priors.

Since the primary GC data we use in this paper have

been marginalized over n_s [27], we should marginalized the CMB distance priors over n_s as well. When marginalized over n_s and $r_s(z_d)$, the inverse covariance matrix of (l_a, R, z_*) from WMAP7 is

$$\text{Cov}_{CMB}^{-1} = \begin{pmatrix} 1.8571 & 25.929 & -1.1433 \\ 25.929 & 5963.3 & -99.319 \\ -1.1433 & -99.319 & 2.9443 \end{pmatrix} \quad (37)$$

CMB data are included in our analysis by adding the following term to the χ^2 of a given model with $p_1 = R(z_*)$, $p_2 = l_a(z_*)$, and $p_3 = z_*$:

$$\chi_{CMB}^2 = \Delta p_i [\text{Cov}_{CMB}^{-1}(p_i, p_j)] \Delta p_j, \quad \Delta p_i = p_i - p_i^{data}, \quad (38)$$

where p_i^{data} are the mean from Eq.(35), and Cov_{CMB}^{-1} is the inverse covariance matrix of $[R(z_*), l_a(z_*), z_*]$ from Eq.(37). Note that $p_4 = n_s$ should be added if the constraints on n_s are included in the GC data. Finally, our Gaussian fit for the pdf of $r_s(z_d)$ should be useful when fitting for BAO peak locations.

D. Gammay-ray Burst Data

We add gammay-ray burst (GRB) data to our analysis, since these are complementary in redshift range to the SN Ia data. We use GRB data in the form of the model-independent GRB distance measurements from Wang (2008c) [40], which were derived from the data of 69 GRBs with $0.17 \leq z \leq 6.6$ from Schaefer (2007) [41].

The GRB distance measurements are given in terms of [40]

$$\bar{r}_p(z_i) \equiv \frac{r_p(z)}{r_p(0.17)}, \quad r_p(z) \equiv \frac{(1+z)^{1/2}}{z} \frac{H_0}{ch} r(z), \quad (39)$$

where $r(z)$ is the comoving distance at z .

The GRB data are included in our analysis by adding the following term to the χ^2 of a given model:

$$\begin{aligned} \chi_{GRB}^2 &= [\Delta \bar{r}_p(z_i)] \cdot (\text{Cov}_{GRB}^{-1})_{ij} \cdot [\Delta \bar{r}_p(z_j)] \\ \Delta \bar{r}_p(z_i) &= \bar{r}_p^{data}(z_i) - \bar{r}_p(z_i), \end{aligned} \quad (40)$$

where $\bar{r}_p(z)$ is defined by Eq.(39). The covariance matrix is given by

$$(\text{Cov}_{GRB})_{ij} = \sigma(\bar{r}_p(z_i))\sigma(\bar{r}_p(z_j)) (\overline{\text{Cov}}_{GRB})_{ij}, \quad (41)$$

where $\overline{\text{Cov}}_{GRB}$ is the normalized covariance matrix from Table 3 of Wang (2008c) [40], and

$$\begin{aligned} \sigma(\bar{r}_p(z_i)) &= \sigma(\bar{r}_p(z_i))^+, \quad \text{if } \bar{r}_p(z) \geq \bar{r}_p(z)^{data}; \\ \sigma(\bar{r}_p(z_i)) &= \sigma(\bar{r}_p(z_i))^- , \quad \text{if } \bar{r}_p(z) < \bar{r}_p(z)^{data}, \end{aligned} \quad (42)$$

where $\sigma(\bar{r}_p(z_i))^+$ and $\sigma(\bar{r}_p(z_i))^-$ are the 68% C.L. errors given in Table 2 of Wang (2008c) [40].

E. Dark energy parametrization

Since we are ignorant of the true nature of dark energy, it is useful to measure the dark energy density function $X(z) \equiv \rho_X(z)/\rho_X(0)$ as a free function of redshift [42–44]. This has the advantage of allowing dark energy models in which $\rho_X(z)$ becomes negative in the future, e.g., the “Big Crunch” models [45, 46], which are precluded if we parametrize dark energy with an equation of state $w_X(z)$ [43].

Here we parametrize $X(z)$ by cubic-splining its values at $z = 1/3, 2/3$, and 1.0 , and assume that $X(z > 1) = X(z = 1)$. For simplicity of notation, we define $X_{0.33} \equiv X(z = 1/3)$, $X_{0.67} \equiv X(z = 2/3)$, and $X_{1.0} \equiv X(z = 1)$. Fixing $X(z > 1)$ reflects the limit of current data, and avoids making assumptions about early dark energy that can be propagated into artificial constraints on dark energy at low z [32, 43].

For comparison with the work of others, we also consider a dark energy equation of state linear in the cosmic scale factor a , $w_X(a) = w_0 + (1 - a)w_a$ [37]. A related parametrization is [34]

$$w_X(z) = w_0(3a - 2) + 3w_{0.5}(1 - a), \quad (43)$$

where $w_{0.5} \equiv w_X(z = 0.5)$. Wang (2008b) [34] showed that $(w_0, w_{0.5})$ are much less correlated than (w_0, w_a) , thus are a better set of parameters to use. We find that $(w_0, w_{0.5})$ converge much faster than (w_0, w_a) in a Markov Chain Monte Carlo (MCMC) likelihood analysis for the same data.

III. RESULTS

We perform a MCMC likelihood analysis [47] to obtain $\mathcal{O}(10^6)$ samples for each set of results presented in this paper. We assume flat priors for all the parameters, and allow ranges of the parameters wide enough such that further increasing the allowed ranges has no impact on the results. The chains typically have worst e-values, defined to be the variance(mean)/mean(variance) of 1/2 chains, much smaller than 0.005, indicating convergence. The chains are subsequently appropriately thinned to ensure independent samples.

In addition to the SN Ia, CMB, GC, and GRB data discussed in Sec.II, we impose a prior of $H_0 = 73.8 \pm 2.4 \text{ km s}^{-1} \text{ Mpc}^{-1}$, from the HST measurements by Riess et al. (2011) [19].

We do *not* assume a flat universe unless specifically noted. In addition to the dark energy parameters described in Sec.IIE, we also constrain cosmological parameters $(\Omega_m, \Omega_k, h, \omega_b)$, where $\omega_b \equiv \Omega_b h^2$. In addition, we marginalize over the SN Ia nuisance parameters $\{\alpha, \beta, \mathcal{M}\}$.

We will present results for dark energy density at $z = 1/3, 2/3$, and 1 , as well as (w_0, w_a) and $(w_0, w_{0.5})$, and a constant dark energy equation of state w .

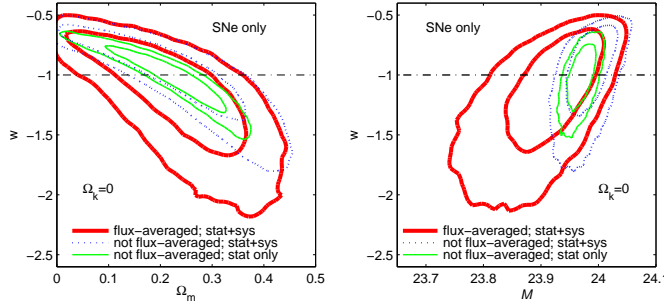


FIG. 6: The 2D marginalized contours of $(w, \Omega_m, \mathcal{M})$ for SNe data (with and without flux-averaging), assuming a flat universe. The contours are at 68% and 95% confidence levels.

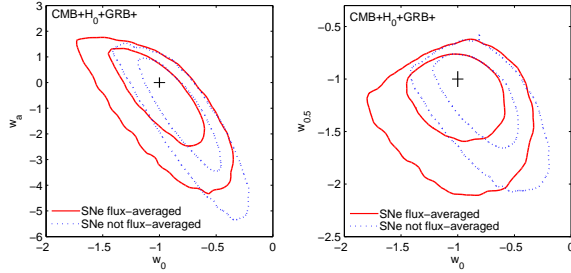


FIG. 7: The 2D marginalized contours of (w_0, w_a) and $(w_0, w_{0.5})$ for SNe data (with and without flux-averaging) combined with CMB, H_0 , and GRB data. The contours are at 68% and 95% confidence levels.

A. The effect of flux-averaging of SNe Ia

Figs.6 shows the 2D marginalized contours of $(w, \Omega_m, \mathcal{M})$, assuming a constant equation of state for dark energy, w , and a flat universe. Note that the inclusion of systematic errors of SNe leads to significantly larger uncertainties in estimated parameters, compared to when only statistical errors of SNe are included. Clearly, flux-averaging (thick solid lines) leads to larger errors on dark energy and cosmological parameters if only SN Ia data are used.

Figs.7-8 show the 2D marginalized contours of (w_0, w_a) and $(w_0, w_{0.5})$ for SNe data combined with CMB, H_0 , and GRB data, without and with GC data (CW2). The solid contours are for flux-averaged SNe, and dotted contours are for SNe without flux-averaging. The SNe data with or without flux-averaging lead to qualitatively consistent results, with flux-averaging expanding the parameter space at $w_0 < -1$, which shifts the bestfit model from $w_0 > -1$ towards $w_0 = -1$, and from $w_a < 0$ towards $w_a = 0$ (it has a smaller impact on $w_{0.5}$ since $w_{0.5}$ is less correlated with w_0 than w_a). Table I tabulates the mean and 68.3% confidence intervals for (w_0, w_a) and $(w_0, w_{0.5})$ corresponding to Figs.7-8.

Fig.9 and Fig.10 are 2D marginalized contours of $(X_{0.33}, X_{0.67}, X_{1.0}, \Omega_m, \Omega_k)$ for SNe data combined with CMB, H_0 , and GRB data, without and with GC data (CW2). The solid contours are for flux-averaged SNe,

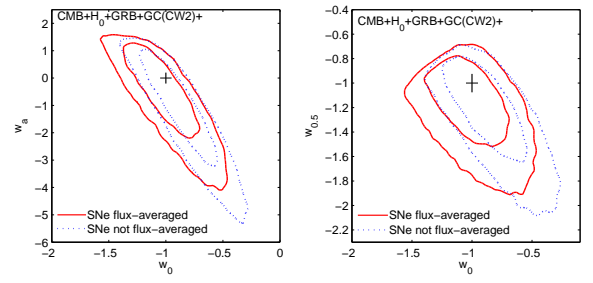


FIG. 8: The 2D marginalized contours of (w_0, w_a) and $(w_0, w_{0.5})$ for SNe data (with and without flux-averaging) combined with galaxy clustering (CW2), CMB, H_0 , and GRB data. The contours are at 68% and 95% confidence levels.

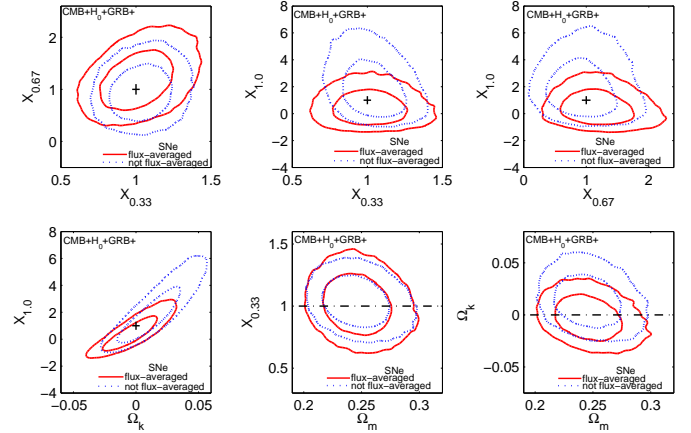


FIG. 9: The 2D marginalized contours of $(X_{0.33}, X_{0.67}, X_{1.0}, \Omega_m, \Omega_k)$ for SNe data (with and without flux-averaging) combined with CMB, H_0 , and GRB data. The contours are at 68% and 95% confidence levels.

and dotted contours are for SNe without flux-averaging. The SNe data with or without flux-averaging lead to qualitatively consistent results, with a shift of the bestfit model towards a cosmological constant; this is the same trend as in the (w_0, w_a) and $(w_0, w_{0.5})$ parametrizations. Note that flux-averaging leads to significantly tighter constraints on the dark energy density at $z = 1$, $X_{1.0}$; this indicates that the impact of flux-averaging increases with redshift, since $(X_{0.33}, X_{0.67}, X_{1.0})$ are only weakly correlated. This is as expected, since the bias in estimated parameters due to weak lensing increases with redshift [26].

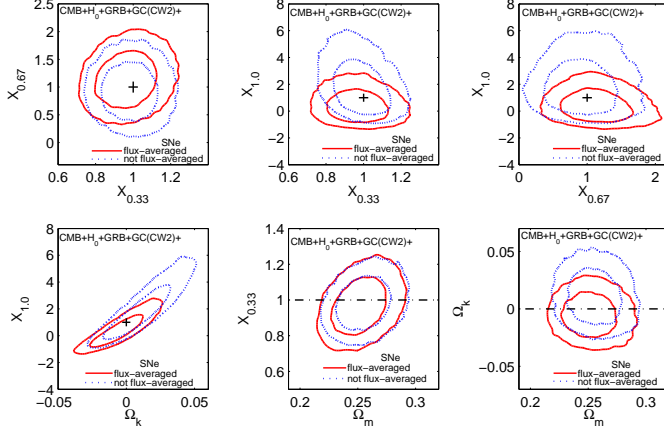
B. Comparison of different galaxy clustering data

We now explore the differences of the various galaxy clustering (GC) measurements in constraining dark energy, assuming a constant equation of state for dark energy, w . Fig.11 shows the 2D marginalized contours of (w, Ω_m, Ω_k) for different GC measurements combined with CMB, H_0 , and GRB data.

The first row of Fig.11 compares the $H(z = 0.35)r_s(z_d)$

TABLE I: Effect of flux-averaging SNe on (w_0, w_a) and $(w_0, w_{0.5})$

	SNe+CMB+ H_0 +GRB			
flux-averaging	w_0	w_a	w_0	$w_{0.5}$
yes	-0.987 (-1.247, -0.727)	-0.780 (-2.046, 0.516)	-0.997 (-1.268, -0.722)	-1.260 (-1.546, -0.965)
no	-0.780 (-1.013, -0.545)	-1.424 (-2.891, 0.045)	-0.783 (-1.023, -0.547)	-1.248 (-1.549, -0.946)
	SNe+CMB+ H_0 +GRB+GC(CW2)			
yes	-0.995 (-1.211, -0.776)	-0.676 (-1.884, 0.566)	-1.000 (-1.216, -0.784)	-1.211 (-1.454, -0.966)
no	-0.832 (-1.061, -0.606)	-1.353 (-2.844, 0.151)	-0.842 (-1.067, -0.615)	-1.266 (-1.559, -0.972)

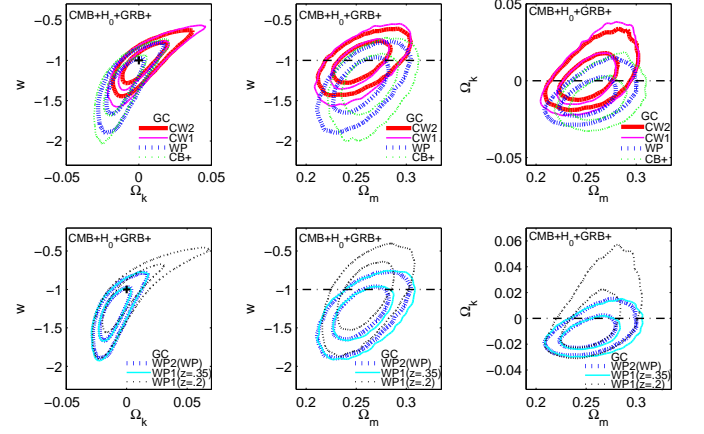
FIG. 10: The 2D marginalized contours of $(X_{0.33}, X_{0.67}, X_{1.0}, \Omega_m, \Omega_k)$ for SNe data (with and without flux-averaging) combined with galaxy clustering (CW2), CMB, H_0 , and GRB data. The contours are at 68% and 95% confidence levels.

and $r_s(z_d)/D_A(z = 0.35)$ measurement by Chuang & Wang (2011) [27] with their $d_{0.35} = r_s(z_d)/D_V(z = 0.35)$ measurement (both from SDSS DR7 LRGs), as well as the $d_{0.2}$ and $d_{0.35}$ measurements by Percival et al. (2010) [28] from SDSS DR7 LRG and main galaxy samples and 2dFGRS, and the $d_{0.6}$ measurement by Blake et al. (2011) from the WiggleZ survey [29] combined with the $d_{0.106}$ measurement by Beutler et al. (2011) from 6dF GRS.

For the Chuang & Wang (2011) [27] GC measurements (CW2 and CW1), the constraints on w are tightened significantly by going from spherically-averaged data (CW1), i.e., $d_{0.35}$, to 2D data (CW2), i.e., $H(z = 0.35)r_s(z_d)$ and $r_s(z_d)/D_A(z = 0.35)$, as indicated by comparing the thin solid contours (CW1) to thick solid contours (CW2) in the first row of Fig.11. This is as expected, as more information from GC is included in CW2 compared to CW1.

Both the Percival et al. (2010) GC measurements (WP) and the combined WiggleZ survey and 6dF GRS measurements (CB+) favor $w < -1$, while the Chuang & Wang (2011) [27] GC measurements favor $w = -1$.

The second row in Fig.11 compares the $d_{0.2}$ and $d_{0.35}$

FIG. 11: The 2D marginalized contours of (w, Ω_m, Ω_k) for different galaxy clustering measurements combined with CMB, H_0 , and GRB data. The contours are at 68% and 95% confidence levels.

measurements by Percival et al. (2010) [28] (WP2), with their measurements of $d_{0.2}$ and $d_{0.35}$ separately. Clearly, most of the constraining power on w comes from $d_{0.35}$. While the $d_{0.2}$ measurement favors $w = -1$, the $d_{0.35}$ measurement favors $w < -1$.

The measurements of $d_{0.35}$ by Chuang & Wang (2011) [27] and Percival et al. (2010) [28] are similar in precision, but differ systematically: $d_{0.35}^{CW} \equiv r_s(z_d)/D_V(z = 0.35) = 0.1161 \pm 0.0034$, while $d_{0.35}^{WP} \equiv r_s(z_d)/D_V(z = 0.35) = 0.1097 \pm 0.0036$. The lower measured value of $d_{0.35}^{WP}$ implies a smaller $H(z = 0.35)$, which in turn implies a more negative w . When combined with CMB, H_0 , and GRB data, $d_{0.35}^{CW}$ favors $w = -1$, while $d_{0.35}^{WP}$ favors $w < -1$. Note that these two measurements used different methods to analyze GC data: Chuang & Wang (2011) used the galaxy correlation function, while Percival et al. (2010) used galaxy power spectrum. It is not surprising that they lead to different distance measurements from GC.

For the rest of this paper, we will present only results using the GC measurements by Chuang & Wang (2011) [27]; these are more conservative as they were derived without assuming CMB priors.

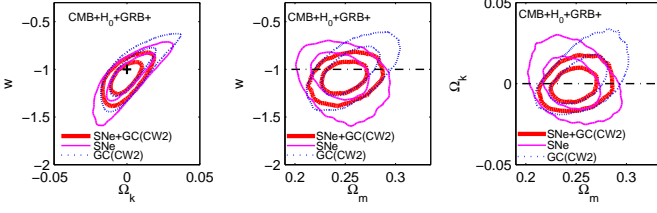


FIG. 12: The 2D marginalized contours of (w, Ω_m, Ω_k) for SNe data (flux-averaged), galaxy clustering measurements (CW2), combined with CMB, H_0 , and GRB data. The contours are at 68% and 95% confidence levels.

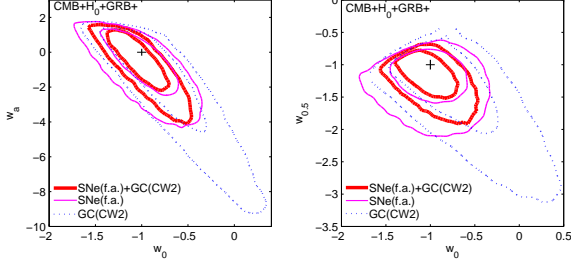


FIG. 13: The 2D marginalized contours of (w_0, w_a) and $(w_0, w_{0.5})$ for SNe data (flux-averaged), galaxy clustering measurements (CW2), combined with CMB, H_0 , and GRB data. The contours are at 68% and 95% confidence levels.

C. Constraints on dark energy and $H(z)$

Figs.12-14 show the 2D marginalized contours of dark energy and cosmological parameters for the three different sets of dark energy parameters: (1) $w_X(z) = w = \text{const.}$; (2) $w_X(z) = w_0 + w_a(1 - a)$, and $w_X(z) = w_0(3a - 2) + 3w_{0.5}(1 - a)$; (3) $X(z) \equiv \rho_X(z)/\rho_X(0)$ given by a cubic spline at $z < 1$ over $X_{z_i} \equiv X(z_i)$, with $z_1 = 1/3$, $z_2 = 2/3$, and $z_3 = 1$, and $X(z > 1) = X(z = 1)$.

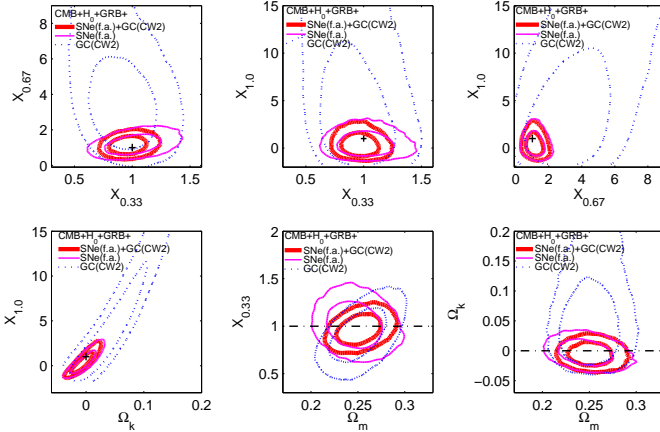


FIG. 14: The 2D marginalized contours of $(X_{0.33}, X_{0.67}, X_{1.0}, \Omega_m, \Omega_k)$ for SNe data (flux-averaged), galaxy clustering measurements (CW2), combined with CMB, H_0 , and GRB data. The contours are at 68% and 95% confidence levels.

Fig.15 shows the dark energy density function $\rho_X(z)$ measured from SNe data (flux-averaged with $dz = 0.07$), galaxy clustering measurements (CW2), combined with CMB, H_0 , and GRB data. The upper panel of Fig.15 shows both $\rho_X(z)$ and $\rho_m(z)$, in units of yoctograms per cubic meter, with 1 yoctogram = 10^{-24} grams. The uncertainties in $X(z)$, $\Omega_X = 1 - \Omega_m - \Omega_k$, and h have been propagated into that of $\rho_X(z)$. The lower panel of Fig.15 shows the corresponding $X(z) = \rho_X(z)/\rho_X(0)$. Fig.16 shows the corresponding cosmic expansion history $H(z)$.

Clearly, given the same priors of CMB, H_0 , and GRB data, SNe lead to much stronger constraints on dark energy than galaxy clustering data at present. Note also that the addition of galaxy clustering data to SN data leads to significantly improved constraints.

Table II gives the dark energy density function $X(z) \equiv \rho_X(z)/\rho_X(0)$ and the cosmic expansion history $H(z)$, as well as $(\Omega_m, \Omega_k, h, \omega_b)$, measured from current data of SNe+GC+CMB+ H_0 +GRB. The $H(z)$ measurements are derived using Eq.(2). Tables III-IV give the normalized covariance matrices of the $X(z)$ and $H(z)$ measurements. Note that both the $X(z)$ and $H(z)$ measurements are only weakly correlated at different redshifts.

To quantify the comparison in dark energy constraints, we can use the general dark energy Figure-of-Merit (FoM) defined by Wang (2008b) [34]

$$\text{FoM} = \frac{1}{\sqrt{\det \text{Cov}(f_1, f_2, \dots, f_N)}} \quad (44)$$

where (f_1, f_2, \dots, f_N) is the set of parameters that have been chosen to parametrize dark energy. The Dark Energy Task Force (DETF) defined the dark energy FoM to be the inverse of the area enclosed by the 95% confidence level contour of (w_0, w_a) [48]. The areas enclosed by contours are difficult to calculate for real data, as these contours can be quite irregular. The definition of Eq.(44) has the advantage of being easy to calculate for either real or simulated data. For $(f_1, f_2) = (w_0, w_a)$, FoM of Eq.(44) is proportional to the FoM defined by the DETF for ideal Gaussian-distributed data, and the same as the relative FoM used by the DETF in Fisher matrix forecasts.

Table V shows the dark energy FoM from SNe (flux-averaged), galaxy clustering measurements (CW2), together with CMB, H_0 , and GRB data, for (w_0, w_a) , $(w_0, w_{0.5})$, and $(X_{0.33}, X_{0.67}, X_{1.0})$.

IV. SUMMARY AND DISCUSSION

We have examined how dark energy constraints from current observational data depend on the analysis methods used: the analysis of Type Ia supernovae (SNe Ia), and that of galaxy clustering data (GC).

We generalize the flux-averaging analysis method of SNe Ia to allow correlated errors of SNe Ia, in order to reduce the systematic bias due to weak lensing of

TABLE II: $X(z)$, $H(z)$, and cosmological parameters estimated from current data with 68.3% C.L. upper and lower uncertainties.

	μ	σ	$\mu + \sigma^-$	$\mu - \sigma^+$
$X(z = 1/3)$	0.969	0.108	0.862	1.077
$X(z = 2/3)$	1.152	0.347	0.812	1.492
$X(z = 1.0)$	0.453	0.863	-0.385	1.284
Ω_m	0.252	0.016	0.236	0.268
Ω_k	-0.0049	0.0131	-0.0180	0.0080
h	0.734	0.019	0.715	0.753
ω_b	0.02234	0.00062	0.02170	0.02290
$H(z = 1/3)/H_0$	1.148	0.040	1.107	1.186
$H(z = 2/3)/H_0$	1.419	0.093	1.328	1.510
$H(z = 1.0)/H_0$	1.511	0.221	1.289	1.731

TABLE III: Normalized covariance matrix of $X(z)$ from current data

	1	2	3
1	1.0000	0.1830	-0.1195
2	0.1830	1.0000	-0.1283
3	-0.1195	-0.1283	1.0000

SNe Ia. We find that flux-averaging leads to larger errors on dark energy and cosmological parameters if only SN Ia data are used (see Fig.6). When SN Ia data (the latest compilation by the SNLS team) are combined with WMAP 7 year results, the latest Hubble constant (H_0) measurement using the HST, and gamma ray burst (GRB) data, flux-averaging of SNe Ia increases the concordance of SNe Ia with other data, and shifts the bestfit cosmological model notably closer to $w = -1$ (see Figs.7-8 and Table I). This leads to significantly tighter constraints on the dark energy density at $z = 1$, and the cosmic curvature Ω_k (see Fig.9). We have made our SN flux-averaging code publicly available at <http://www.nhn.ou.edu/~wang/SNcode/>.

We find that given the same priors (CMB+ H_0 +GRB), both the Percival et al. (2010) GC measurements [28] (WP: $d_{0.2}$ and $d_{0.35}$) and the combined WiggleZ survey and 6dF GRS measurements [29, 30] (CB+: $d_{0.6}$ and $d_{0.106}$) favor $w < -1$ ¹, while the Chuang & Wang (2011) GC measurements [27] (CW2: $H(z = 0.35)r_s(z_d)$ and $r_s(z_d)/D_A(z = 0.35)$) favor $w = -1$ (see Fig.11). This could be due to the difference in the analysis methods used to derive these GC measurements. We find that the GC measurements by Chuang & Wang (2011) are consistent with SN Ia data (which favor $w = -1$), and tighten

the dark energy constraints significantly when combined with SN data (see Fig.12-14).

For the convenience of future work, we have derived Gaussian fits to the probability distributions of a set of CMB parameters, $[R(z_*), l_a(z_*), z_*, n_s, r_s(z_d)]$ (see Figs.1-5), that summarize the WMAP7 data, as well as well their covariance matrix. Note that while $[R(z_*), l_a(z_*), z_*]$ are sufficient for summarizing the CMB priors when n_s dependence has been marginalized over in GC analysis, $[R(z_*), l_a(z_*), z_*, n_s]$ need to be used when the constraints on n_s from GC are included (as will be the case for future GC data). We find that $r_s(z_d)$ gives redundant information, its measurement cannot be used in the CMB priors unless it is used to replace $l_a(z_*)$. Also, our Gaussian fit for the pdf of $r_s(z_d)$ from WMAP7 can be useful when fitting for BAO peaks in GC data analysis.

We find that current data are fully consistent with a cosmological constant and a flat universe, consistent with the latest findings by others (see, e.g., [18, 50–56]). Since the uncertainties remain large, a deviation from a cosmological constant is far from being ruled out (see Fig.15).

At present, SN data provide much stronger constraints than GC data (see Table V). This will change when ambitious galaxy surveys are carried out from space in the future [57, 58]. We can expect dramatic progress in our measurement and understanding of dark energy in the next decade or so.

Acknowledgements We are grateful to Alex Conley for communicating details of the SNLS data, to Ei-

¹ Similar results were found by [49, 50] using Percival et al. (2010) GC measurements [28].

TABLE IV: Normalized covariance matrix of $H(z)/H_0$ from current data

	1	2	3
1	1.0000	0.2657	0.0727
2	0.2657	1.0000	-0.0575
3	0.0727	-0.0575	1.0000

TABLE V: Dark energy FoM from current data

CMB+ H_0 +GRB+	FoM _r ($\{X_i\}$)	$\sigma(w_0)$	$\sigma(w_{0.5})$	$r_{w_0, w_{0.5}}$	FoM _r ($w_0, w_{0.5}$)	$\sigma(w_0)$	$\sigma(w_a)$	r_{w_0, w_a}	FoM _r (w_0, w_a)
SNe	18.61	0.27	0.33	-0.12	11.02	0.27	1.32	-0.70	3.98
GC	0.44	0.44	0.59	-0.74	5.76	0.39	2.40	-0.89	2.31
SNe+GC	32.00	0.22	0.27	-0.51	19.80	0.22	1.24	-0.84	6.74

ichihiro Komatsu for making the covariance matrix for $[R(z_*), l_a(z_*), z_*, r_s(z_d), n_s]$ he derived from WMAP 7 year data available, and to Max Tegmark for suggesting the presentation of $\rho_X(z)$ in the upper panel of Fig.15. We acknowledge the use of CAMB and CosmoMC. YW

and CHC are supported in part by DOE grant DE-FG02-04ER41305. PM is supported in part by the L'Oreal UK and Ireland Fellowship For Women in Science, and by the University of Sussex.

-
- [1] Riess, A. G., *et al.*, 1998, *Astron. J.*, 116, 1009
[2] Perlmutter, S. *et al.*, 1999, *ApJ*, 517, 565
[3] Copeland, E. J., Sami, M., Tsujikawa, S., *IJMPD*, 15 (2006), 1753
[4] Ruiz-Lapuente, P., *Class. Quantum. Grav.*, 24 (2007), 91
[5] Ratra, B., Vogeley, M. S., *arXiv:0706.1565* (2007)
[6] Frieman, J., Turner, M., Huterer, D., *ARAA*, 46, 385 (2008)
[7] Caldwell, R. R., & Kamionkowski, M., *arXiv:0903.0866*
[8] Uzan, J.-P., *arXiv:0908.2243*
[9] Wang, Y., *Dark Energy*, Wiley-VCH (2010)
[10] Li, M., *et al.*, 2011, *arXiv:1103.5870*
[11] Blake, C.; Glazebrook, K., 2003, *ApJ*, 594, 665
[12] Seo, H; Eisenstein, D J 2003, *ApJ*, 598, 720
[13] Hu, W., 2002, *PRD*, 66, 083515
[14] Jain, B. & Taylor, A. *PRL*, 91, 141302 (2003)
[15] Amati, L., *et al.* 2002, *A&A*, 390, 81
[16] Bloom, J. S., Frail, D. A., & Kulkarni, S. R. 2003, *ApJ*, 594, 674
[17] Schaefer, B. E., 2003, *ApJ*, 583, L71
[18] Komatsu, E., *et al.* 2011, *Astrophys.J.Suppl.*, 192, 18
[19] Riess, A. G., *et al.*, 2011, *ApJ*, 730, 119
[20] Wang, Y., *Journal of Cosmology and Astroparticle Physics*, 05, 021 (2008).
[21] Simpson, F., & Peacock, J.A. 2010, *Phys Rev D*, 81, 043512
[22] Conley, A., *et al.*, 2011, *Astrophys.J.Suppl.*, 192, 1
[23] Hui, L., & Greene, P.B., *PRD*, 73, 123526 (2006)
[24] Wang, Y., *ApJ* 536, 531 (2000)
[25] Wang, Y., & Mukherjee, P. 2004, *ApJ*, 606, 654
[26] Wang, Y., *JCAP*, 03, 005 (2005)
[27] Chuang, C.-H.; and Wang, Y., *arXiv:1102.2251*
[28] Percival, W.J., *et al.* 2010, *MNRAS*, 401, 2148
[29] Blake, C., *et al.* 2011, *MNRAS*, 415, 2892
[30] Beutler, F., *et al.*, 2011, *arXiv:1106.3366*, *MNRAS*, in press
[31] Page, L., *et al.* 2003, *ApJS*, 148, 233
[32] Wang, Y., & Mukherjee, P., *PRD*, 76, 103533 (2007)
[33] Li, H., *et al.*, *ApJ*, 683, L1 (2008)
[34] Wang, Y., 2008b, *Phys. Rev. D* 77, 123525
[35] Hu, W., & Sugiyama, N. 1996, *ApJ*, 471, 542
[36] Eisenstein, D. & Hu, W. 1998, *ApJ*, 496, 605
[37] Chevallier, M., & Polarski, D. 2001, *Int. J. Mod. Phys. D* 10, 213
[38] Komatsu, E., “wmap_prior_for_bao.pdf” at <http://gyudon.as.utexas.edu/~komatsu/wmap7/>
[39] Wang, Y., *PRD*, 80, 123525 (2009)
[40] Wang, Y., 2008b, *PRD*, 78, 123532
[41] Schaefer, B. E., 2007, *ApJ*, 660, 16
[42] Wang, Y., and Garnavich, P. 2001, *ApJ*, 552, 445
[43] Wang, Y., & Tegmark, M. 2004, *Phys. Rev. Lett.*, 92, 241302
[44] Wang, Y., & Freese, K. 2006, *Phys.Lett. B* 632, 449 (astro-ph/0402208)
[45] Linde, A. D., “Inflation And Quantum Cosmology,” in *Three hundred years of gravitation*, (Eds.: Hawking, S.W. and Israel, W., Cambridge Univ. Press, 1987), 604-630.
[46] Wang, Y.; Kratochvil, J. M.; Linde, A.; & Shmakova, M., *JCAP* 0412 (2004) 006
[47] Lewis, A., & Bridle, S. 2002, *PRD*, 66, 103511
[48] Albrecht, A.; Bernstein, G.; Cahn, R.; Freedman, W. L.; Hewitt, J.; Hu, W.; Huth, J.; Kamionkowski, M.; Kolb, E.W.; Knox, L.; Mather, J.C.; Staggs, S.; Suntzeff, N.B., Report of the Dark Energy Task Force, astro-ph/0609591
[49] Escamilla-Rivera, C.; *et al.*, 2011, *JCAP*, 09, 003
[50] Li, X.-D., *et al.*, *JCAP* 07 (2011) 011

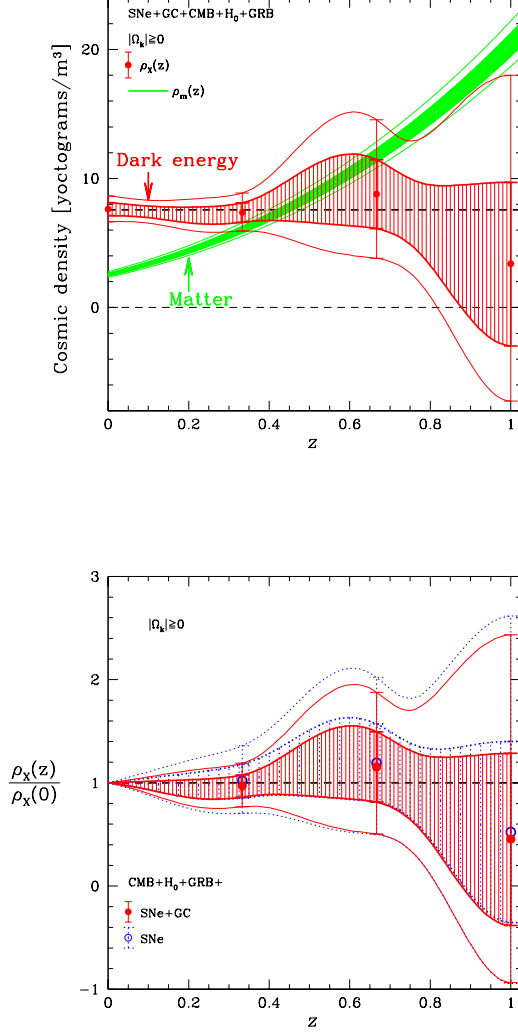


FIG. 15: Dark energy density function $\rho_X(z)$ measured from SNe data (flux-averaged with $dz = 0.07$), galaxy clustering measurements (CW2), combined with CMB, H_0 , and GRB data. The contours are at 68% and 95% confidence levels. The upper panel shows both $\rho_X(z)$ and $\rho_m(z)$ in units of yoctograms per cubic meter, with 1 yoctogram = 10^{-24} grams. The lower panel shows the corresponding $X(z) = \rho_X(z)/\rho_X(0)$.

- [51] Bean, R.; Tangmatitham, M., PRD, 81, 083534
- [52] Chen, Y.; Ratra, B., arXiv:1106.4294
- [53] Dossett, J.N.; Moldenhauer, J.; Ishak, M., 2011, PRD, 84, 023012
- [54] Holsclaw, T.; et al., arXiv:1104.2041
- [55] Liang, N.; Wu, P.-X.; Zhu, Z.-H., 2011, RAA, 11, 1019
- [56] Wang, S.; Li, X.-D.; Li, M., 2011, PRD, 83, 023010
- [57] Cimatti, A., et al., Experimental Astronomy, 23, 39 (2009)
- [58] Wang, Y., et al., MNRAS, 409, 737 (2010)

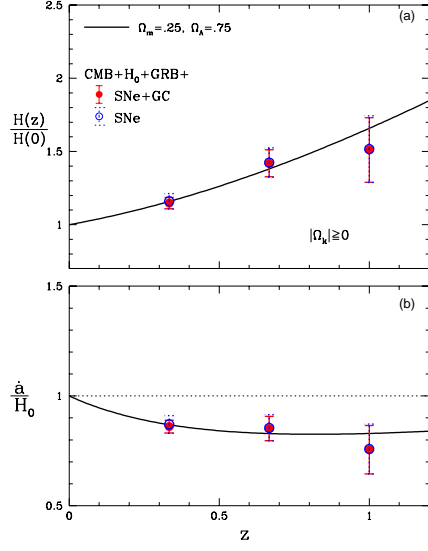


FIG. 16: The cosmic expansion history $H(z)$ measured from SNe data (flux-averaged with $dz = 0.07$), galaxy clustering measurements (CW2), combined with CMB, H_0 , and GRB data. The error bars indicate the 68.3% confidence level ranges.